A PARTICLE METHOD FOR THE SEMICLASSICAL LIMIT OF THE SCHRÖDINGER EQUATION AND THE VLASOV-POISSON EQUATIONS [*]

SHI JIN[†] AND DONGMING WEI[‡]

Abstract. When using standard deterministic particle methods, point values of the computed solutions have to be recovered from their singular particle approximations by using some smoothing procedure. The choice of the smoothing procedure is rather flexible. Moreover, there is always a parameter associated with the smoothing procedure: if this parameter is too large, the numerical solution loses its accuracy; if it is too small, oscillation appears. No explicit formula has been given on how to choose this parameter.

In this paper, we develop a particle method for the semiclassical limit of the Schrödinger equation and the Vlasov-Poisson equations, in which we use the property of *conservation of charge*, which was studied in [30], to construct the density. This method avoids the recovery step of the particle methods, thus it is simpler and more accurate. In particular it gives more accurate field quantities. Consequently, we apply this method to the Vlasov-Poisson equations, which yields more accurate density and electric field in each time step. We carry out numerical experiments in both one and two dimensions for the Schrödinger equation and Vlasov-Poisson equations to verify the method. Some comparisons with other particle methods are also made.

Key words. Schrödinger equation, Vlasov-Poisson equation, particle method

AMS subject classifications. 65M75, 35L45, 35Q40

1. Introduction. In this paper, we propose a novel numerical method for the Liouville equation

$$f_t + H_{\boldsymbol{\xi}} \cdot \nabla_{\mathbf{x}} f - H_{\mathbf{x}} \cdot \nabla_{\boldsymbol{\xi}} f = 0 \,, \quad t > 0 \,, \quad \mathbf{x}, \boldsymbol{\xi} \in \mathbb{R}^d \,. \tag{1.1}$$

The function $f(t, \mathbf{x}, \boldsymbol{\xi})$ is the density distribution of particles depending on position $\mathbf{x}$, time t and velocity $\boldsymbol{\xi}$. The solution to this problem is a superposition of delta functions of variable weight concentrating on the bi-characteristic strips of the equation which is governed by the Hamiltonian system

$$\frac{\partial \mathbf{x}}{dt} = \nabla_{\boldsymbol{\xi}} H \,, \quad \frac{\partial \boldsymbol{\xi}}{dt} = -\nabla_{\mathbf{x}} H \,, \quad \text{with} \quad H(\mathbf{x}, \boldsymbol{\xi}) = \frac{1}{2} |\boldsymbol{\xi}|^2 + V(\mathbf{x}),$$

where $V(\mathbf{x})$ is the potential function. The moments of f yield the physical observables, namely, density $\rho(\mathbf{x}, t) = \int_{\mathbb{R}^d} f(t, \mathbf{x}, \mathbf{v}) d\mathbf{v}$ and momentum $\rho(\mathbf{x}, t) \mathbf{u}(\mathbf{x}, t) = \int_{\mathbb{R}^d} f(t, \mathbf{x}, \mathbf{v}) \mathbf{v} d\mathbf{v}$, where $\mathbf{u}(\mathbf{x}, t)$ is the velocity.

We will also consider the Vlasov-Poisson equations which are just (1.1) with potential V given by

$$\Delta_{\mathbf{x}} V = \int_{\mathbb{R}^d} f(t, \mathbf{x}, \mathbf{v}) dv =: \rho(\mathbf{x}, t) \,. \tag{1.2}$$

Equation (1.1) provides a phase space description of the semiclassical limit of the Schödinger equation [9, 19]:

$$i\hbar \partial_t \psi^{\hbar} = -\frac{\hbar^2}{2} \Delta \psi^{\hbar} + V(\mathbf{x}) \psi^{\hbar}, \qquad \mathbf{x} \in \mathbb{R}^d, \tag{1.3}$$

[†]Department of Mathematics, University of Wisconsin, Madison WI 53706, jin@math.wisc.edu.

[‡]Division of Applied Mathematics, Brown University, Providence, RI 02912, weidongmmm@hotmail.com.

where $\psi^\hbar$ is the complex-valued wave function, $\hbar$ the reduced Planck constant. In this setting, one typically considers the Schrödinger equation (1.3) with the WKB initial data of the form $\psi(\mathbf{x},0) = A_0(\mathbf{x})\exp(iS_0(\mathbf{x})/\hbar)$ with smooth S_0. In the semiclassical limit $\hbar \to 0$, the Wigner transform of ψ is f that satisfies the Liouville equation (1.1) with the mono-kinetic initial data:

$$f(0,\mathbf{x},\boldsymbol{\xi}) = |A_0(\mathbf{x})|^2 \delta(\boldsymbol{\xi} - \nabla_\mathbf{x} S_0(\mathbf{x})) =: \rho_0(\mathbf{x})\delta(\boldsymbol{\xi} - \nabla_\mathbf{x} S_0(\mathbf{x})). \qquad (1.4)$$

The Vlasov-Poisson equations arise in semiconductor device modeling [23] and plasma physics [18]. For mathematical analysis of this system see [2, 20, 31, 21, 22], while for numerical methods see [11, 1, 8, 28, 29].

When one closes (1.1) and (1.4) with the moments–which give the density and momentum of particles–the moment system satisfies the pressureless gas dynamics equations, which develop delta-shock solutions in finite time, corresponding to caustics in geometric optics. Beyond the caustics, only the multi-valued solutions are physically relevant [27, 12]. The computation of multi-valued solutions in geometrical optics and semiclassical limit of the Schrödinger equation, using the Liouville equation (1.1) in the Eulerian level set framework, has been an active area of research in recent years, see for examples [24, 3, 17, 14]. Recent overviews of this subject can be found in [7, 13].

We focus our attention on the Lagrangian particle methods. When using a particle method, one has to recover the point values of the computational solutions from their singular particle approximations which are the Dirac delta functions. The most common approach is to approximate the Dirac delta function by its convolution with a smooth kernel, see, e.g., [5, 26, 6]. For a comparison between the convolution recovery and other redistribution recovery strategies, see [4]. In this paper, we propose a more accurate recovery strategy. In [30], an analysis on the 1D Vlasov-Poisson equations with electron sheet initial data used the following conservative quantity

$$\int_{\Upsilon(0)} f(0,\mathbf{x},\boldsymbol{\xi})d\boldsymbol{\xi}d\mathbf{x} = \int_{\Upsilon(t)} f(t,\mathbf{x},\boldsymbol{\xi})d\boldsymbol{\xi}d\mathbf{x}, \quad \forall\,\Upsilon(0) \subset \mathbb{R}^{2d},\ \forall t, \qquad (1.5)$$

where

$$\Upsilon(t) = \left\{ (\mathbf{x},\boldsymbol{\xi})(t,\mathbf{x_0},\boldsymbol{\xi_0}) \left| \frac{d\mathbf{x}}{ds} = \boldsymbol{\xi},\ \frac{d\boldsymbol{\xi}}{ds} = -\nabla_\mathbf{x} V, \mathbf{x}(0) = \mathbf{x}_0, \boldsymbol{\xi}(0) = \boldsymbol{\xi}_0, (\mathbf{x_0},\boldsymbol{\xi_0}) \in \Upsilon(0) \right. \right\}$$

are the particle trajectories. We call (1.5) the *conservation of charge.* In this paper, we propose to use this theoretical property to formulate a particle method. This method allows one to get a more accurate density ρ, which is only a postprocessing for (1.1) of course, but for equations with a field, such as the Vlasov-Poisson equations (1.1) and (1.2), it provides a more accurate (time-dependent) potential–and consequently the electric field $E = -\nabla_\mathbf{x} V$– at each time step, thus enhances the numerical accuracy overall in long time.

In fact, our formulation allows us to treat more general initial data than (1.4). Let C be a curve in the x-ξ space. Let $C(\alpha) = \left\{ \left(x(\alpha), \xi(\alpha) \right) \middle| \alpha \in \Omega \right\}$ be a parameterized form of C. We first make the following definition:

DEFINITION 1.1. *The function $\vartheta_C(x,\xi)$ is a surface measure supported on the curve C, defined by*

$$\int_{\mathbb{R}^2} \psi(x,\xi)\vartheta_C(x,\xi)d\xi dx = \int_\Omega \psi\big(x(\alpha),\xi(\alpha)\big)\left|\frac{dC(\alpha)}{d\alpha}\right|d\alpha, \quad \forall\psi \in C_0^\infty(\mathbb{R}^2),$$

where $\left|\dfrac{dC(\alpha)}{d\alpha}\right| d\alpha = \sqrt{x'(\alpha)^2 + \xi'(\alpha)^2}\,d\alpha$ *is the infinitesimal arc length.*

The initial data

$$f(0, x, \xi) = \rho_0(x)\left|\dfrac{dC(x)}{dx}\right|^{-1}\vartheta_C, \tag{1.6}$$

is the so-called electron sheet initial data [21]. In the semiclassical limit problem, $f(0, x, \xi) = h(x, \xi)\vartheta_C$ allows the initial data to be multi-valued, thus are more general than the mono-kinetic initial data (1.4).

This paper is organized as follows. In section 2, we derive a formula of weak solutions of the Liouville equations with singular (measure-valued) initial data (1.6). In section 3, we describe a numerical density reconstruction method based on the conservation of charge (1.5) for one, two and general space dimensions. In section 4, we extend the method to the Vlasov-Poisson equations. In section 5, 1D and 2D numerical examples are given for the Liouville equation and Vlasov-Poisson equations, and comparisons are made with classical particle methods. This paper is concluded in section 6.

2. Weak solution of the Liouville equation with measure-valued initial data. We construct weak solutions of the one-dimensional Liouville equations with measure-valued initial data in section 2.1. Then we extend the result to the multi-dimensional case.

2.1. One space dimension. Since Definition 1.1 will be used in our weak solution formulation, we will first elaborate on this definition.

2.1.1. On Definition 1.1. Definition 1.1 is independent of the choice of the parametrization α. Without loss of generality, we assume $\alpha \in \Omega = (a, b)$. Let $C(\beta) = \left\{ \left(\widetilde{x}(\beta), \widetilde{\xi}(\beta)\right) \Big| \beta \in (r, s) \right\}$ be another parameterized form of C. Then there exists a unique monotonic function g such that $(x(g(\beta)), \xi(g(\beta))) = (\widetilde{x}(\beta), \widetilde{\xi}(\beta))$. Therefore

$$\int_a^b \psi\Big(x(\alpha), \xi(\alpha)\Big)\sqrt{x'(\alpha)^2 + \xi'(\alpha)^2}\,d\alpha$$
$$= \int_{g^{-1}(a)}^{g^{-1}(b)} \psi\Big(x(g(\beta)), \xi(g(\beta))\Big)\sqrt{x'(g(\beta))^2 + \xi'(g(\beta))^2}\,d(g(\beta))$$
$$= \int_{g^{-1}(a)}^{g^{-1}(b)} \psi\Big(\widetilde{x}(\beta), \widetilde{\xi}(\beta)\Big)\sqrt{(\widetilde{x}'(\beta)^2 + \widetilde{\xi}'(\beta)^2)/g'(\beta)^2}\,g'(\beta)\,d\beta$$
$$= \int_{g^{-1}(a)}^{g^{-1}(b)} \operatorname{sign}(g'(\beta))\psi\Big(\widetilde{x}(\beta), \widetilde{\xi}(\beta)\Big)\sqrt{(\widetilde{x}'(\beta)^2 + \widetilde{\xi}'(\beta)^2)}\,d\beta$$
$$= \int_r^s \psi\Big(\widetilde{x}(\beta), \widetilde{\xi}(\beta)\Big)\sqrt{(\widetilde{x}'(\beta)^2 + \widetilde{\xi}'(\beta)^2)}\,d\beta.$$

REMARK 2.1. The mono-kinetic initial data (1.4) is a special case (in the weak sense) of the more general initial data (which allows the initial data to be multi-valued)

$$f(0, x, \xi) = \rho_0(x)\left|\dfrac{dC(x)}{dx}\right|^{-1}\vartheta_C, \tag{2.1}$$

with

$$C(x) = \Big\{ \big(x, \xi(x)\big) = \big(x, \nabla_x S_0(x)\big) \Big| x \in (-\infty, \infty) \Big\}. \tag{2.2}$$

We verify it below: $\forall \psi \in C_0^\infty(\mathbb{R}^2)$,

$$\int_{\mathbb{R}^2} \psi(x,\xi)\rho_0(x)\delta(\xi - \nabla_x S_0(x))d\xi dx = \int_{-\infty}^{\infty} \psi\big(x, \nabla_x S_0(x)\big)\rho_0(x)dx,$$

$$\int_{\mathbb{R}^2} \psi(x,\xi)\rho_0(x)\left|\frac{dC(x)}{dx}\right|^{-1}\vartheta_C d\xi dx = \int_{-\infty}^{\infty} \psi\big(x, \nabla_x S_0(x)\big)\rho_0(x)\left|\frac{dC(x)}{dx}\right|^{-1}\left|\frac{dC(x)}{dx}\right|dx.$$

Thus they are identical for all test functions, hence (1.4) and (2.1) are equivalent in the weak sense.

A general measure supported on the curve $C(\alpha)$ has the form $h(x,\xi)\vartheta_C$. By Definition 1.1, $\forall \psi \in C_0^\infty(\mathbb{R}^2)$,

$$\int_{\mathbb{R}^2} \psi(x,\xi)h(x,\xi)\vartheta_C(x,\xi)d\xi dx = \int_{\Omega} \psi\big(x(\alpha),\xi(\alpha)\big)h\big(x(\alpha),\xi(\alpha)\big)\left|\frac{dC(\alpha)}{d\alpha}\right|d\alpha. \quad (2.3)$$

Notice that for function h, only the value on the curve C matters, that is, only $h(x(\alpha),\xi(\alpha)) =: h(\alpha)$ matters. Therefore, we denote the measure as $h(x,\xi)\vartheta_C =: h(\alpha)\vartheta_{C(\alpha)}$.

2.1.2. Weak solutions and conservation of charge. DEFINITION 2.1. *A function f is a weak solution of (1.1) if it satisfies the weak form of (1.1) which is given by*

$$\int_0^\infty \int_{\mathbb{R}^2} (\psi_t f + f\xi \cdot \nabla_x \psi - f\nabla_x V \cdot \nabla_\xi \psi)dx d\xi dt = 0, \quad \forall \psi \in C_0^\infty(\mathbb{R}^2 \times \mathbb{R}^+). \quad (2.4)$$

We now give a formula for weak solutions of the 1D Liouville equations, and conservation of charge, in the following theorem.

THEOREM 2.2. *Consider (1.1) subject to the delta function initial data, i.e., a measure supported on a curve $C(\alpha,0) = \left\{\big(x(\alpha,0),\xi(\alpha,0)\big)\big| \alpha \in \Omega\right\}$ which has the following form $f(0,x,\xi) = \varrho_0(\alpha)\left|\frac{dC(\alpha,0)}{d\alpha}\right|^{-1}\vartheta_{C(\alpha,0)}$. Denote the solution of the initial value problem of the Hamiltonian system*

$$\frac{dx}{dt} = \xi, \quad \frac{d\xi}{dt} = -\nabla_x V, \quad x(0) = x(\alpha,0), \quad \xi(0) = \xi(\alpha,0), \quad (2.5)$$

by $\big(x(\alpha,t),\xi(\alpha,t)\big)$. Then

$$f(t,x,\xi) = \varrho_0(\alpha)\left|\frac{dC(\alpha,t)}{d\alpha}\right|^{-1}\vartheta_{C(\alpha,t)} \quad (2.6)$$

is a weak solution to (1.1), which is a delta function supported on the curve

$$C(\alpha,t) = \left\{\big(x(\alpha,t),\xi(\alpha,t)\big)\big| \alpha \in \Omega\right\}.$$

Moreover, for every interval (β,γ), let $\Lambda(t) = \left\{\big(x(\alpha,t),\xi(\alpha,t)\big)\big| \alpha \in (\beta,\gamma)\right\}$, then

$$\int_{\mathbb{R}^2} f(0,x,\xi)I_{\Lambda(0)}dx d\xi = \int_{\mathbb{R}^2} f(t,x,\xi)I_{\Lambda(t)}dx d\xi = \int_\beta^\gamma \varrho_0(\alpha)d\alpha, \quad \forall t, \quad (2.7)$$

where I_Λ is the characteristic function supported on Λ. (2.7) is referred to "conservation of charge" [30].

Proof. For all $\psi \in C_0^\infty\left(\mathbb{R} \times \mathbb{R} \times [0, T]\right)$, since $\frac{dx(\alpha,t)}{dt} = \xi(\alpha, t)$, $\frac{d\xi(\alpha,t)}{dt} = -\nabla_x V$, it follows that

$$\frac{d\psi(x(\alpha,t), \xi(\alpha,t), t)}{dt} = \frac{\partial\psi(x(\alpha,t), \xi(\alpha,t), t)}{\partial t} + \xi(\alpha, t) \cdot \nabla_x \psi(x(\alpha,t), \xi(\alpha,t), t)$$
$$- \nabla_x V \cdot \nabla_\xi \psi(x(\alpha,t), \xi(\alpha,t), t).$$

Therefore, for f given by (2.6)

$$\int_0^T \int_{\mathbb{R}^2} (\psi_t f + f\xi \cdot \nabla_x \psi - f\nabla_x V \cdot \nabla_\xi \psi) dx d\xi dt$$
$$= \int_0^T \int_{\mathbb{R}} \Big[\frac{\partial\psi(x(\alpha,t), \xi(\alpha,t), t)}{\partial t} + \xi(\alpha, t) \cdot \nabla_x \psi(x(\alpha,t), \xi(\alpha,t), t)$$
$$- \nabla_x V \cdot \nabla_\xi \psi(x(\alpha,t), \xi(\alpha,t), t) \Big] \varrho_0(\alpha) \left| \frac{dC(\alpha,t)}{d\alpha} \right|^{-1} \left| \frac{dC(\alpha,t)}{d\alpha} \right| d\alpha dt$$
$$= \int_0^T \int_{\mathbb{R}} \frac{d\psi(x(\alpha,t), \xi(\alpha,t), t)}{dt} \varrho_0(\alpha) d\alpha dt = 0.$$

We used (2.3) in the first equality above. $\square$

2.1.3. Multi-valued solutions and physical observables. We now explain the relationship between $f(t, x, \xi)$ and the physical observables, which gives rise to the multi-valued solutions. First, for the mono-kinetic initial data

$$f(0, x, \xi) = \rho_0(x)\delta(\xi - \nabla_x S_0(x)) = \rho_0(x) \left| \frac{dC(x)}{dx} \right|^{-1} \vartheta_C,$$

$\rho_0(x)$ is the local density, that is, $\rho_0(x) = \int_{-\infty}^{\infty} f(0, x, \xi) d\xi$. For every fixed x, $f(0, x, \xi)$ is a Dirac-delta function with respect to ξ supported at the point $\nabla_x S_0(x)$.

In the general case, where $f(t, x, \xi)$ is a measure supported on $C(\alpha, t)$, and $C(\alpha, t)$ is not necessarily a graph in the x-ξ plane, we claim the following theorem

THEOREM 2.3. *Consider a solution of (1.1) with the form (2.6), $\forall w \in \mathbb{R}$, such that $x(\alpha, t) = w$ has finitely many solutions which are denoted by $\alpha_1(w), \alpha_2(w), \ldots, \alpha_k(w)$, that is*

$$x(\alpha_1(w), t) = x(\alpha_2(w), t) = \cdots = x(\alpha_k(w), t) = w, \qquad (2.8)$$

and

$$\left. \frac{\partial x}{\partial \alpha} \right|_{\alpha = \alpha_j(w)} \neq 0, \quad j = 1, \ldots, k, \qquad (2.9)$$

there exists $\kappa > 0$, such that

$$f(t, z, \xi) = \sum_{j=1}^{k} \varrho_0(\alpha_j(z)) \left| \frac{\partial x}{\partial \alpha} \right|_{\alpha = \alpha_j(z)}^{-1} \delta(\xi - \xi(\alpha_j(z))), \qquad \forall z \in (w - \kappa, w + \kappa). \quad (2.10)$$

Proof. For every fixed w that satisfies (2.8) and (2.9), there exists a $\tau > 0$, such that $x(\alpha, t)$ is one-to-one on $(\alpha_j(w) - \tau, \alpha_j(w) + \tau)$, $j = 1, \ldots, k$. Denote

$$g_j(\alpha) = x(\alpha, t), \qquad \alpha \in (\alpha_j(w) - \tau, \alpha_j(w) + \tau), \qquad j = 1, \ldots, k. \qquad (2.11)$$
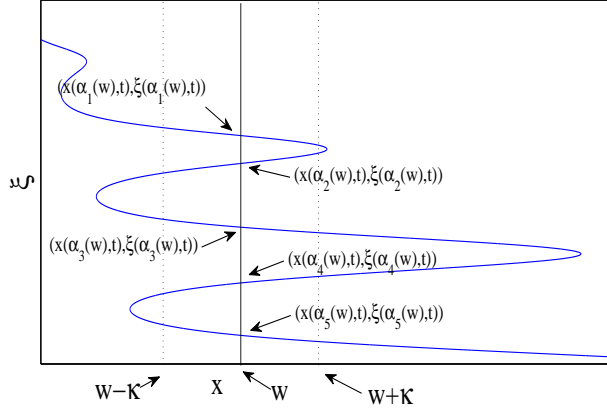
Fig. 2.1: A simple illustration of (2.12)

Consequently, there exists a $\kappa > 0$, such that $\forall z \in (w - \kappa, w + \kappa)$, the equation $x(\alpha, t) = z$ yields exactly k solutions $\alpha_1(z), \ldots, \alpha_k(z)$, such that

$$\alpha_j(z) \in (\alpha_j(w) - \tau, \alpha_j(w) + \tau), \qquad j = 1, \ldots, k. \qquad (2.12)$$

See Fig 2.1. We now prove $\forall z \in (w - \kappa, w + \kappa)$, $\forall \psi \in C_0^\infty(\mathbb{R}^2)$,

$$\int_{-\infty}^{\infty} \psi(z, \xi) f(t, z, \xi) d\xi = \int_{-\infty}^{\infty} \psi(z, \xi) \left(\sum_{j=1}^{k} \varrho_0(\alpha_j(z)) \left| \frac{\partial x}{\partial \alpha} \right|_{\alpha = \alpha_j(z)}^{-1} \delta(\xi - \xi(\alpha_j(z))) \right) d\xi, \qquad (2.13)$$

and then (2.10) follows. The left hand side of (2.13) can be reformulated as

$$\frac{\partial}{\partial z} \int_{-\infty}^{z} \int_{-\infty}^{\infty} \psi(x, \xi) f(t, x, \xi) d\xi dx = \frac{\partial}{\partial z} \int_{w-\kappa}^{z} \int_{-\infty}^{\infty} \psi(x, \xi) f(t, x, \xi) d\xi dx.$$

Plugging (2.6) into the above, and using the fact that $(x(\alpha, t), \xi(\alpha, t)) \in (w - \kappa, z) \times (-\infty, \infty)$ if and only if $\alpha \in \bigcup_{j=1}^{k} \left(g_j^{-1}(w - \kappa), g_j^{-1}(z) \right)$, we obtain

$$\int_{-\infty}^{\infty} \psi(z, \xi) f(t, z, \xi) d\xi = \frac{\partial}{\partial z} \int_{w-\kappa}^{z} \int_{-\infty}^{\infty} \psi(x, \xi) \varrho_0(\alpha) \left| \frac{dC(\alpha)}{d\alpha} \right|^{-1} \vartheta_C d\xi dx$$

$$= \frac{\partial}{\partial z} \int_{-\infty}^{\infty} \int_{-\infty}^{\infty} I_{(w-\kappa,z) \times (-\infty,\infty)} \psi(x, \xi) \varrho_0(\alpha) \left| \frac{dC(\alpha)}{d\alpha} \right|^{-1} \vartheta_C d\xi dx$$

$$= \frac{\partial}{\partial z} \left(\sum_{j=1}^{k} \text{sign}(g_j^{-1}(z) - g_j^{-1}(w - \kappa)) \int_{g_j^{-1}(w-\kappa)}^{\alpha_j(z) = g_j^{-1}(z)} \psi\Big(x(\alpha), \xi(\alpha) \Big) \varrho_0(\alpha) d\alpha \right)$$

$$= \sum_{j=1}^{k} \text{sign}(g_j^{-1}(z) - g_j^{-1}(w - \kappa)) \frac{\partial \big(g_j^{-1}(z) \big)}{\partial z} \psi\Big(x(\alpha_j(z)), \xi(\alpha_j(z)) \Big) \varrho_0(\alpha_j(z))$$

Since it is possible that $g_j^{-1}(z) < g_j^{-1}(w - \kappa)$, we multiply each integral in the above expression by the sign of $(g_j^{-1}(z) - g_j^{-1}(w - \kappa))$ to make it correct. Recall that $g_j(\alpha) = x(\alpha, t)$ on $(\alpha_j(w) - \tau, \alpha + \tau)$, therefore $|\frac{\partial x}{\partial \alpha}|_{\alpha = \alpha_j(z)}^{-1} = \text{sign}(g_j^{-1}(z) - g_j^{-1}(w -$

$\kappa)) \frac{\partial \left(g_j^{-1}(z) \right)}{\partial z}$. We find

$$
\int_{-\infty}^{\infty} \psi(z,\xi) f(t,z,\xi) d\xi = \sum_{j=1}^{k} \left| \frac{\partial x}{\partial \alpha} \right|_{\alpha=\alpha_j(z)}^{-1} \psi\Big(x(\alpha_j(z)), \xi(\alpha_j(z)) \Big) \varrho_0(\alpha_j(z))
$$

$$
= \sum_{j=1}^{k} \psi\Big(z, \xi(\alpha_j(z)) \Big) \left| \frac{\partial x}{\partial \alpha} \right|_{\alpha=\alpha_j(z)}^{-1} \varrho_0(\alpha_j(z))
$$

$$
= \int_{-\infty}^{\infty} \psi(z,\xi) \left(\sum_{j=1}^{k} \varrho_0(\alpha_j(z)) \left| \frac{\partial x}{\partial \alpha} \right|_{\alpha=\alpha_j(z)}^{-1} \delta(\xi - \xi(\alpha_j(z))) \right) d\xi.
$$

□

REMARK 2.2. If there are infinitely but countably many solutions of $x(\alpha) = z$, then there exists $\frac{\partial x}{\partial \alpha}|_{\alpha=\alpha_j(z)} = 0$, and the local density $\rho(z,t) = \infty$. If the set $\{\alpha | x(\alpha,t) = z\}$ is not discrete, i.e., its measure in $\mathbb{R}$ is greater than 0, then the local density $\rho(z,t)$ is a Dirac mass. Points where $\rho = \infty$ correspond to caustics.

We define $\widetilde{\rho}(\alpha,t) := |\partial x(\alpha,t)/\partial \alpha|^{-1} \varrho_0(\alpha)$. Then

$$
f(t,z,\xi) = \sum_{j=1}^{k} \widetilde{\rho}(\alpha_j(z),t) \delta\Big(\xi - \xi(\alpha_j(z),t) \Big). \tag{2.14}
$$

Here each term on the right hand side of (2.14) corresponds to one phase of the so-called multi-valued solution, whose summation, f, is a weak solution to (1.1) corresponding to the semiclassical limit of the Schrödinger equation [27, 12]. The physical observables at $x = z$ are

$$
\text{density:} \quad \rho(z,t) = \int_{-\infty}^{\infty} f(t,z,\xi) d\xi = \sum_{j=1}^{k} \widetilde{\rho}(\alpha_j(z),t), \tag{2.15}
$$

$$
\text{momentum:} \quad \rho u^m(z,t) = \int_{-\infty}^{\infty} \xi^m f(t,z,\xi) d\xi = \sum_{j=1}^{k} \widetilde{\rho}(\alpha_j(z),t) \xi(\alpha_j(z),t)^m, \tag{2.16}
$$

which are superposition of multi-valued solutions. Suppose $x(\alpha,t)$ is one-to-one on (β,γ). Denote its inverse on (β,γ) by $\alpha(z) = x^{-1}(z)$. Let $\Lambda = \left\{ \big(x(\alpha,t), \xi(\alpha,t) \big) \,\middle|\, \alpha \in (\beta,\gamma) \right\}$, then

$$
\int_{-\infty}^{\infty} \int_{-\infty}^{\infty} I_\Lambda f(t,z,\xi) d\xi dx = \int_{\beta}^{\gamma} \varrho_0(\alpha) \left| \frac{dC(\alpha,t)}{d\alpha} \right|^{-1} \left| \frac{dC(\alpha,t)}{d\alpha} \right| d\alpha
$$

$$
= \int_{\beta}^{\gamma} \varrho_0(\alpha) d\alpha = \int_{x(\beta)}^{x(\gamma)} \varrho_0(x^{-1}(z)) \left(\frac{\partial x^{-1}}{\partial z} \right) dz \qquad \alpha(z) = x^{-1}(z) \tag{2.17}
$$

$$
= \text{sign}(x(\gamma) - x(\beta)) \int_{x(\beta)}^{x(\gamma)} \widetilde{\rho}(\alpha(z),t) dz.
$$

Let $M(\varpi) = \int_0^\varpi \varrho_0(\alpha) d\alpha$, then

$$
\text{sign}(x(\gamma) - x(\beta)) \int_{x(\beta,t)}^{x(\gamma,t)} \widetilde{\rho}(\alpha(z),t) dz = M(\gamma) - M(\beta) = \int_{\beta}^{\gamma} \varrho_0(\alpha) d\alpha. \tag{2.18}
$$

We summarize the result here. To calculate the physical observables, one needs the following information: (i) the curve $C(\alpha, t)$ and (ii) $\widetilde{\rho}(\alpha, t)$. Then to find the moment $\rho u^m(z, t)$ at z, we solve $x(\alpha, t) = z$, suppose there are k solutions $\alpha_1, \ldots, \alpha_k$, then $\rho u^m(z, t) = \sum_{j=1}^{k} \widetilde{\rho}(\alpha_j, t) \xi^m(\alpha_j, t)$, the superposition of moments of each branch of the multi-valued momentum. The detailed numerical algorithm is given in Section 3.

2.2. Multi-dimensional case. Now, we extend Definition 1.1 to surface measure supported on a hyperplane in multi-dimensional space.

DEFINITION 2.4. *Let P be a hyperplane in the $\mathbf{x}$-$\boldsymbol{\xi}$ space, $\mathbf{x} \in \mathbb{R}^d$, $\boldsymbol{\xi} \in \mathbb{R}^d$. Let $P(\boldsymbol{\alpha}) = \left\{ \left(\mathbf{x}(\boldsymbol{\alpha}), \boldsymbol{\xi}(\boldsymbol{\alpha}) \right) \Big| \boldsymbol{\alpha} \in \Omega \right\}$ be a parameterized form of P. The function $\eta_P(\mathbf{x}, \boldsymbol{\xi})$ is a surface measure supported on the hyperplane P, defined by*

$$\int_{\mathbf{R}^{2d}} \psi(\mathbf{x}, \boldsymbol{\xi}) \eta_P(\mathbf{x}, \boldsymbol{\xi}) d\boldsymbol{\xi} d\mathbf{x} = \int_{\Omega} \psi\left(\mathbf{x}(\boldsymbol{\alpha}), \boldsymbol{\xi}(\boldsymbol{\alpha})\right) \frac{dY(\boldsymbol{\alpha})}{d\boldsymbol{\alpha}} d\boldsymbol{\alpha}, \quad \forall \psi \in C_0^\infty(\mathbb{R}^{2d}), \quad (2.19)$$

where $\int_\Lambda \dfrac{dY(\boldsymbol{\alpha})}{d\boldsymbol{\alpha}} d\boldsymbol{\alpha}$ is the area of the hyperplane $P(\boldsymbol{\alpha} \in \Lambda)$, $\forall \Lambda \subset \Omega$.

REMARK 2.3. It is easy to verify that definition 2.4 is independent of the choice of the parametrization $\boldsymbol{\alpha}$.

In general, the hyperplane has dimension $0 \leq k \leq 2d$, with $\Omega \subset \mathbb{R}^k$. The mono-kinetic initial data (1.4) is a special case of (2.19), where the hyperplane has dimension d. More precisely, (1.4) is equivalent, in the weak sense to a measure supported on a hyperplane $P(\mathbf{x}, \nabla_\mathbf{x} S_0(\mathbf{x}))$ such that the local density $\int_{\mathbf{R}^d} f d\boldsymbol{\xi} = \rho_0(\mathbf{x})$, that is,

$$f(0, \mathbf{x}, \boldsymbol{\xi}) = \rho_0(\mathbf{x}) \left(\frac{dY}{d\mathbf{x}}\right)^{-1} \eta_P(\mathbf{x}, \boldsymbol{\xi}),$$

in the weak sense. We verify it below: $\forall \psi \in C_0^\infty(\mathbb{R}^{2d})$,

$$\int_{\mathbf{R}^{2d}} \psi(\mathbf{x}, \boldsymbol{\xi}) \rho_0(\mathbf{x}) \delta(\boldsymbol{\xi} - \nabla_\mathbf{x} S_0(\mathbf{x})) d\boldsymbol{\xi} d\mathbf{x} = \int_{\mathbf{R}^d} \psi\left(\mathbf{x}, \nabla_\mathbf{x} S_0(\mathbf{x})\right) \rho_0(\mathbf{x}) d\mathbf{x},$$

$$\int_{\mathbf{R}^{2d}} \psi(\mathbf{x}, \boldsymbol{\xi}) \rho_0(\mathbf{x}) \left(\frac{dY}{d\mathbf{x}}\right)^{-1} \eta_P(\mathbf{x}, \boldsymbol{\xi}) d\boldsymbol{\xi} d\mathbf{x} = \int_{\mathbf{R}^d} \psi\left(\mathbf{x}, \nabla_\mathbf{x} S_0(\mathbf{x})\right) \rho_0(\mathbf{x}) \left(\frac{dY}{d\mathbf{x}}\right)^{-1} \left(\frac{dY}{d\mathbf{x}}\right) d\mathbf{x}.$$

Thus

$$\int_{\mathbf{R}^{2d}} \psi(\mathbf{x}, \boldsymbol{\xi}) \rho_0(\mathbf{x}) \delta(\boldsymbol{\xi} - \nabla_\mathbf{x} S_0(\mathbf{x})) d\boldsymbol{\xi} d\mathbf{x} = \int_{\mathbf{R}^{2d}} \psi(\mathbf{x}, \boldsymbol{\xi}) \rho_0(\mathbf{x}) \left(\frac{dY}{d\mathbf{x}}\right)^{-1} \eta_P(\mathbf{x}, \boldsymbol{\xi}) d\boldsymbol{\xi} d\mathbf{x}.$$

Also in general, we do not require P to be a graph in $\mathbf{x} - \boldsymbol{\xi}$ space with dimension d. Let $g(\mathbf{x}, \boldsymbol{\xi}) = p(\mathbf{x}, \boldsymbol{\xi}) \eta_P$ be a surface measure supported on P. Then the value of p on P determines the measure g. More precisely, $p(\boldsymbol{\alpha}) := p(\mathbf{x}(\boldsymbol{\alpha}), \boldsymbol{\xi}(\boldsymbol{\alpha})), \boldsymbol{\alpha} \in \Omega$, determines g. Therefore, for $P(\boldsymbol{\alpha}) = \left\{ \left(\mathbf{x}(\boldsymbol{\alpha}), \boldsymbol{\xi}(\boldsymbol{\alpha}) \right) \Big| \boldsymbol{\alpha} \in \Omega \right\}$, we simply denote g as $g(\boldsymbol{\alpha}) = p(\boldsymbol{\alpha}) \eta_{P(\boldsymbol{\alpha})}$. Similar to the 1D case, we define a weak solution of (1.1) for $x \in \mathbb{R}^d$.

DEFINITION 2.5. *A function f is a weak solution of (1.1) if it satisfies the weak form of (1.1) which is given by*

$$\int_0^T \int_{\mathbb{R}^{2d}} (\psi_t f + f\boldsymbol{\xi} \cdot \nabla_\mathbf{x} \psi - f \nabla_\mathbf{x} V \cdot \nabla_{\boldsymbol{\xi}} \psi) d\mathbf{x} d\boldsymbol{\xi} dt = 0.$$

Equipped with this definition, we now give a formula for weak solutions of the multi-D Liouville equations in the following theorem.

THEOREM 2.6. *Consider (1.1) with measure initial data $f_0 = \varrho_0(\boldsymbol{\alpha})\left|\dfrac{dY(\boldsymbol{\alpha},0)}{d\boldsymbol{\alpha}}\right|^{-1}\eta_{P(\boldsymbol{\alpha},0)}$, i.e., a measure supported on a hyperplane with dimension k with the form $P(\boldsymbol{\alpha},0) = (\mathbf{x}_0(\boldsymbol{\alpha}),\boldsymbol{\xi}_0(\boldsymbol{\alpha}))$, $\boldsymbol{\alpha} \in \Omega \subset \mathbb{R}^k$. Denote the solution of the initial value problem to the Hamiltonian system*

$$\frac{d\mathbf{x}}{dt} = \boldsymbol{\xi}, \quad \frac{d\boldsymbol{\xi}}{dt} = -\nabla_{\mathbf{x}}V, \quad \mathbf{x}(0) = \mathbf{x}_0(\boldsymbol{\alpha}), \quad \boldsymbol{\xi}(0) = \boldsymbol{\xi}_0(\boldsymbol{\alpha}),$$

by $\big(\mathbf{x}(\boldsymbol{\alpha},t),\boldsymbol{\xi}(\boldsymbol{\alpha},t)\big)$. Then a measure supported on the hyperplane $P(\boldsymbol{\alpha},t) = (\mathbf{x}(\boldsymbol{\alpha},t),\boldsymbol{\xi}(\boldsymbol{\alpha},t))$, $\boldsymbol{\alpha} \in \Omega$,

$$f(t,\mathbf{x},\boldsymbol{\xi}) = \varrho_0(\boldsymbol{\alpha})\left|\frac{dY(\boldsymbol{\alpha},t)}{d\boldsymbol{\alpha}}\right|^{-1}\eta_{P(\boldsymbol{\alpha},t)},$$

is a weak solution to (1.1) with the given initial data. Let $P_\Lambda(t) = \{\big(\mathbf{x}(\boldsymbol{\alpha},t),\boldsymbol{\xi}(\boldsymbol{\alpha},t)\big)\,|\,\boldsymbol{\alpha} \in \Lambda \subset \mathbb{R}^k\}$. Then

$$\int_{\mathbb{R}^{2d}} f(0,\mathbf{x},\boldsymbol{\xi})I_{P_\Lambda(0)}d\mathbf{x}d\boldsymbol{\xi} = \int_{\mathbb{R}^{2d}} f(t,\mathbf{x},\boldsymbol{\xi})I_{P_\Lambda(t)}d\mathbf{x}d\boldsymbol{\xi}, \quad \forall\Lambda \subset \Omega, \quad \forall t. \qquad (2.20)$$

The proof of this theorem is similar to the proof of Theorem 2.2, so we omit the details.

Consider the Liouville equation with initial data (1.4), that is $\Omega \subset \mathbb{R}^d$. Similar to the one-dimensional case, denote $\widetilde{\rho}(\boldsymbol{\alpha},t) := \left|\dfrac{\partial\mathbf{x}(\boldsymbol{\alpha},t)}{\partial\boldsymbol{\alpha}}\right|^{-1}\varrho_0(\boldsymbol{\alpha})$, then $f(t,\mathbf{x},\boldsymbol{\xi})$ can be rewritten as

$$f(t,\mathbf{z},\boldsymbol{\xi}) = \sum_{j=1}^{k}\widetilde{\rho}(\boldsymbol{\alpha}_j(\mathbf{z}),t)\delta\Big(\boldsymbol{\xi} - \boldsymbol{\xi}(\boldsymbol{\alpha}_j(\mathbf{z}),t)\Big), \qquad (2.21)$$

where $\boldsymbol{\alpha}_1(\mathbf{z}),\ldots,\boldsymbol{\alpha}_k(\mathbf{z})$ are solutions of $\mathbf{x}(\boldsymbol{\alpha},t) = \mathbf{z}$. Moreover, if $\mathbf{x}(\boldsymbol{\alpha},t)$ is one-to-one on $\boldsymbol{\alpha} \in \Omega_1 \subset \Omega$, then

$$\int_{\mathbf{x}(\Omega_1)} \widetilde{\rho}(\mathbf{x}^{-1}(\mathbf{z}),t)d\mathbf{z} = \int_{\Omega_1} \varrho_0(\boldsymbol{\alpha})d\boldsymbol{\alpha}.$$

3. The detailed numerical implementation.

3.1. The one-dimensional numerical implementation. We now describe the numerical details for the one-dimensional Liouville equation. A key idea is to use the conservation of charge (2.7); or rather (2.18). Suppose the initial data is given by

$$f(0,x,\xi) = \varrho_0(\alpha)\left|\frac{dC(\alpha,0)}{d\alpha}\right|^{-1}\vartheta_{C(\alpha,0)}. \qquad (3.1)$$

Without loss of generality, we assume $\alpha \in (0,1)$.

Step 1. Let $\alpha_j = j/N$, $j = 0,\ldots,N$, be the initial partition of the curve $C(\alpha,0)$.
Step 2. Evaluate the initial charge $m_j = \int_{\alpha_{j-1}}^{\alpha_j} \varrho_0(\alpha)d\alpha$, $j = 1,\ldots,N$, numerically by some quadrature rule or analytically if possible.

Step 3. Solve $\dfrac{dx_j(t)}{dt} = \xi_j, \quad \dfrac{d\xi_j(t)}{dt} = -V_x, \quad x_j(0) = x(\alpha_j, 0), \quad \xi_j(0) = \xi(\alpha_j, 0),$
numerically to obtain $x_j(T), u_j(T), j = 0, \ldots, N.$

Step 4. Approximate $C(\alpha, T)$. For example, if a piecewise linear approximation is used, one gets

$$x(\alpha, T) = x_{j-1}(T) + \frac{\alpha - \alpha_{j-1}}{N}\big(x_j(T) - x_{j-1}(T)\big), \quad \alpha \in (\alpha_{j-1}, \alpha_j), \qquad (3.2a)$$

$$\xi(\alpha, t) = \xi_{j-1}(T) + \frac{\alpha - \alpha_{j-1}}{N}\big(\xi_j(T) - \xi_{j-1}(T)\big), \quad j = 1, \ldots, N. \qquad (3.2b)$$

This also gives a multi-valued solution of the velocity $\widetilde{u}$, that is,

$$\widetilde{u}(x(\alpha, t), t) = \xi(\alpha, t), \quad \alpha \in (0, 1). \qquad (3.3)$$

$\widetilde{u}$ can be multi-valued since it is possible that $x(\beta_1, t) = x(\beta_2, t)$ for $\beta_1 \neq \beta_2$.
Step 5. By (2.18)

$$\text{sign}(x(\alpha_{j+1}, T) - x(\alpha_j, T)) \int_{x(\alpha_j, T)}^{x(\alpha_{j+1}, T)} \widetilde{\rho}(\alpha(z), t)dz = M(\alpha_{j+1}) - M(\alpha_j) = m_j.$$

We use a constant to approximate $\widetilde{\rho}(\alpha, T)$ on $\alpha \in (\alpha_j, \alpha_{j+1})$. That is,

$$\widetilde{\rho}(\alpha, T) \approx \frac{m_j}{|x(\alpha_{j+1}, T) - x(\alpha_j, T)|}, \qquad \alpha \in (\alpha_j, \alpha_{j+1}).$$

Similar to $\widetilde{u}$, $\widetilde{\rho}$ gives a multi-valued solution of density. The (single valued) position density, namely the zeroth moment defined in (2.15) is given by

$$\rho(y, T) = \sum_{j=0}^{N-1} \frac{m_j}{|x(\alpha_{j+1}, T) - x(\alpha_j, T)|} I_{(x(\alpha_j, T), x(\alpha_{j+1}, T))}(y). \qquad (3.4)$$

Step 6. Compute any desired physical observables by using the results of Step 4 and 5. For example, from definition (2.16)

$$\rho(y, T)u(y, T) = \sum_{p=1}^{k} \widetilde{\rho}(\alpha_p(y), T)\xi(\alpha_p(y), T),$$

where $\alpha_p(y)$ are solutions of $x(\alpha, T) = y$. By (3.2), if $y \in (x(\alpha_j, T), x(\alpha_{j+1}, T))$, then $\alpha = \frac{y - x_j(T)}{x_{j+1}(T) - x_j(T)}N + \alpha_j$ is a solution of $x(\alpha, T) = y$, and $\xi(\alpha, t) = \xi_j(T) + \frac{(y - x_j(T))(\xi_{j+1}(T) - \xi_j(T))}{x_{j+1}(T) - x_j(T)}$. Therefore

$$\rho(y, T)u(y, T) = \sum_{j=0}^{N-1} \frac{m_j I_{(x(\alpha_j, T), x(\alpha_{j+1}, T))}(y)}{|x(\alpha_{j+1}, T) - x(\alpha_j, T)|}\Big(\xi_j(T) + \frac{(y - x_j(T))(\xi_{j+1}(T) - \xi_j(T))}{x_{j+1}(T) - x_j(T)}\Big).$$

3.2. A detailed implementation of the 2D Algorithm. In this subsection, we give a detailed numerical implementation for the 2D Liouville equation with initial data (1.4). Numerical methods for the higher dimensional Liouville equation can be constructed similarly.

Without loss of generality, assume $\mathbf{x} = (x, y) \in [0, 1] \times [0, 1], \boldsymbol{\xi} \in \mathbb{R}^2$.

Step 1. Given mesh size $\Delta x = \Delta y = 1/N$. Denote $\mathbf{x}(j,l) = (x_j, y_l)$.

Step 2. There are N^2 cells. Denote the cell $(x_j, x_{j+1}) \times (y_l, y_{l+1})$ by $\Omega_k(0)$, where $k = (j+1+lN)$. Since the elementary elements in 2D are triangles, we further split $\Omega_k(0)$ into two parts $\Omega_{k1}(0)$ and $\Omega_{k2}(0)$, where $\Omega_{k1}(0)$ is the triangle with vertices $\mathbf{x}(j,l), \mathbf{x}(j+1,l), \mathbf{x}(j,l+1)$, and $\Omega_{k2}(0)$ is the triangle with vertices $\mathbf{x}(j,l+1), \mathbf{x}(j+1,l), \mathbf{x}(j+1,l+1)$. See figure 3.2 for an illustration. Evaluate the initial charge
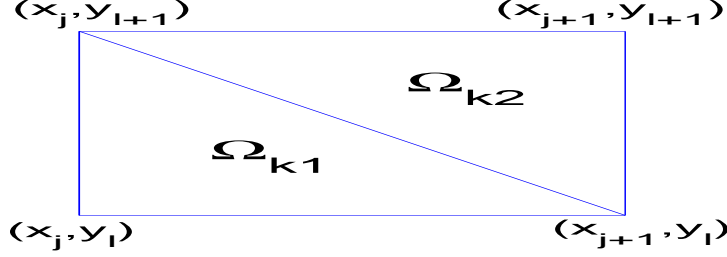
Fig. 3.1: 2D mesh with triangles Ω_{k1} and Ω_{k2}.

$$m_{kq} = \int\int_{\Omega_{kq}} \rho_0(x,y)dxdy \quad k = 1, \ldots, N^2, \quad q = 1,2,$$

numerically by some quadrature rule or analytically if possible.

Step 3. Solve numerically $\dfrac{d\mathbf{x}_{jl}(t)}{dt} = \boldsymbol{\xi}_{jl}, \dfrac{d\boldsymbol{\xi}_{jl}(t)}{dt} = -\nabla_{\mathbf{x}} V$, subject to the initial data $\mathbf{x}_{jl}(0) = (x_j, y_l), \boldsymbol{\xi}_{jl}(0) = \nabla_{\mathbf{x}} S_0(\mathbf{x}_{jl}(0))$, to obtain $\mathbf{x}_{jl}(T), \boldsymbol{\xi}_{jl}(T), j = 0, \ldots, N$, $l = 0, \ldots, N$.

Step 4. Apply the linear interpolation to approximate velocity on $\Omega_{kq}(T)$. More precisely, denote the vertices of Ω_{kq} by $\mathbf{a}, \mathbf{b}, \mathbf{c}$, and the velocity at them are $\mathbf{u_a}, \mathbf{u_b}, \mathbf{u_c}$ respectively. Then for every $\mathbf{x} \in \Omega_{kq}$, one can decompose $\mathbf{x} - \mathbf{a}$ uniquely as $\mathbf{x} - \mathbf{a} = \mu(\mathbf{b} - \mathbf{a}) + \nu(\mathbf{c} - \mathbf{a})$, here (μ, ν) can be solved analytically, and interpolate $\boldsymbol{\xi}(\mathbf{x}, t) = \mathbf{u_a} + \mu(\mathbf{u_b} - \mathbf{u_a}) + \nu(\mathbf{u_c} - \mathbf{u_a})$. This gives a multi-valued solution of velocity $\tilde{\mathbf{u}}$ at time T. Denote $\boldsymbol{\xi}(\mathbf{x}, t)$ on Ω_{kq} by $\boldsymbol{\xi}_{kq}(\mathbf{x}, t)$.

Step 5. Denote the area of the triangle $\Omega_{kq}(T)$ by $A_{kq}(T)$. Let $\tilde{\rho}(\boldsymbol{\alpha}, T) = \dfrac{m_{kq}}{A_{kq}(T)}$ on (associated with) $\Omega_{kq}(T)$. This gives a multi-valued solution of density at time T. The (single valued) position density, defined in (2.21) with $m = 0$ then follows

$$\rho(\mathbf{x}, T) = \sum_{q=1}^{2} \sum_{k=1}^{N^2} \frac{m_{kq}}{A_{kq}(T)} I_{\Omega_{kq}(T)}(\mathbf{x}) \tag{3.5}$$

Step 6. Compute any desired physical variables by using the result of Steps 4 and 5. For example, from (2.21) with $m = 1$,

$$\rho(\mathbf{x}, T)u(\mathbf{x}, T) = \sum_{q=1}^{2} \sum_{k=1}^{N^2} \frac{m_{kq}}{A_{kq}(T)} I_{\Omega_{kq}(T)}(\mathbf{x}) \boldsymbol{\xi}_{kq}(\mathbf{x}, T).$$

REMARK 3.1. One can apply any higher order numerical method in Steps 3, 4 and 5. In addition to its high efficiency and accuracy, a major advantage of the method

is that it gives very accurate numerical solutions around caustics. The reason is: the particles become automatically dense when caustic develops, and the total charge inside any cell around the caustic is calculated at $t = 0$. For classical particle methods, one has to apply some smoothing procedure to recover point values of the computed solutions from their singular particle approximations, therefore, even the particles are dense around the caustics, the smoothing procedure smears the solution. For details of the smoothing procedures, see Section 5.1. Another side product is that we obtain the multi-valued solution rather than the single valued physical observables.

REMARK 3.2. For a 2D problem, when using (3.5) to calculate the local density ρ on a mesh $\{\mathbf{y}_{ij}\}$, one needs to identify whether $\mathbf{y}_{ij}$ is inside a triangle or not many times. We apply the following fast test method. Denote the vertices of the triangle Ω_{kq} ($q = 1$ or 2) by $\mathbf{a}, \mathbf{b}, \mathbf{c}$, where $\mathbf{a} = (a_1, a_2)$, $\mathbf{b} = (b_1, b_2)$ and $\mathbf{c} = (c_1, c_2)$. Denote $x_{\min} = \min\{a_1, b_1, c_1\}$, $x_{\max} = \max\{a_1, b_1, c_1\}$, $y_{\min} = \min\{a_2, b_2, c_2\}$, $y_{\max} = \max\{a_2, b_2, c_2\}$. Then for every $\mathbf{y}_{ij} \in \mathbb{R}^2$, we first test whether $\mathbf{y}_{ij} \in (x_{\min}, x_{\max}) \times (y_{\min}, y_{\max})$. If so, we decompose $\mathbf{y}_{ij} - \mathbf{a}$ as $\mathbf{y}_{ij} - \mathbf{a} = \mu(\mathbf{b} - \mathbf{a}) + \nu(\mathbf{c} - \mathbf{a})$, then $\mathbf{y}_{ij}$ is inside the triangle Ω_{kq} if and only if $0 < \mu < 1$, $0 < \nu < 1$ and $\mu + \nu < 1$. This procedure greatly enhances the numerical method for the Vlasov-Poisson equation to be present in the next section, since there one needs to construct ρ at every time step.

4. The Vlasov-Poisson equations. We can apply the new method to the Vlasov-Poisson equations

$$f_t + \mathbf{v} \cdot \nabla_{\mathbf{x}} f - \mathbf{E}(\mathbf{x}, t) \cdot \nabla_{\mathbf{v}} f = 0, \tag{4.1a}$$

$$\Delta_{\mathbf{x}} V = \int_{\mathbb{R}^d} f(\mathbf{x}, \mathbf{v}, t) dv =: \rho(\mathbf{x}, t), \quad E = -\nabla_{\mathbf{x}} V, \tag{4.1b}$$

here $E(\mathbf{x}, t)$ is the electric field, V the potential.

For example, for the 2D Vlasov-Poisson equations, in each time step t to $t + \Delta t$, we do the following:

(i) Choose a uniform mesh $\{\mathbf{y}_{ij}\}$ on $\mathbf{x}$-plane, $1 \le i, j \le N$. The initial particles are located at the mesh points: $\mathbf{x}_{ij}(0) = \mathbf{y}_{ij}$.

(ii) solve the bi-characteristic equations numerically $\dfrac{d\mathbf{x}_{ij}(t)}{dt} = \boldsymbol{\xi}_{ij}$, $\dfrac{d\boldsymbol{\xi}_{ij}(t)}{dt} = -E$, to get particle positions and velocities $\mathbf{x}_{ij}(t + \Delta t)$, $\boldsymbol{\xi}_{ij}(t + \Delta t)$;

(iii) use (3.5) to calculate the local density on *uniform mesh points* $\{\mathbf{y}_{ij}\}$ at time $t + \Delta t$; then use the standard five-point center difference scheme to solve the Poisson equation (4.1b) to get the potential $V(t + \Delta t, \mathbf{y}_{ij})$; take finite difference of $V(t + \Delta t, \mathbf{y}_{ij})$ to get $E(t + \Delta t, \mathbf{y}_{ij})$;

(iv) use the linear interpolation to get E on *particle positions* $\mathbf{x}_{ij}(t + \Delta t)$, which will be used in (ii) in the next time step.

REMARK 4.1. The particle number is $M = (N+1)^2$. In step (iii), the computational cost for evaluating the single valued position density ρ on uniform mesh points $\mathbf{y}_{ij}$ of our method and all other particle methods are of the same order $O(M^2)$. In step (iv), the computational cost for evaluating E on particle positions of all methods are of order $O(M)$. Although the computational cost for all methods have the same order, our method is much faster than the previous particle methods in practice. We show a comparison in a 2D numerical example in section 5.2.

5. Numerical examples. We carry out one and two dimensional numerical experiments in this section. In these examples, we compare numerical solutions obtained

by our method with solutions obtained by previous particle methods. The main difference between our proposed method and the previous particle methods is that the latter have to apply some smoothing procedures to recover point value of the numerical solution from the singular particle approximation. For reader's convenience, in Section 5.1 we briefly describe three smoothing procedures that have been studied in [4], and refer to [4] and references therein for more details.

In all examples, we solve the ODEs by the forward Euler method, although one can use any other higher order methods. The initial charge m_j was computed by the Matlab subroutines QUAD and QUAD2D, which approximate the integral by using recursive adaptive Simpson quadrature.

5.1. The smoothing procedures of particle methods. To use the particle method, one first replaces the initial data $f(0, \mathbf{x}, \boldsymbol{\xi}) = \rho_0(\mathbf{x})\delta(\boldsymbol{\xi} - \mathbf{u}_0(\mathbf{x}))$ with a singular particle approximation. More precisely, one decomposes the computational domain Ω into M nonintersecting domains $\Omega = \Omega_1 \bigcup \cdots \bigcup \Omega_M$. Then particles with masses $\int_{\Omega_i} \rho_0(\mathbf{x})d\mathbf{x}$ are placed initially at $\mathbf{x}_i(0)$, where $\mathbf{x}_i(0)$ are the coordinates of the centers of mass of Ω_i. The initial velocities of the particles are taken to be $\mathbf{u}_0(\mathbf{x}_i(0)) =: (u_{i1}, u_{i2}, \ldots, u_{id})(0)$. That is, one replaces $f(0, \mathbf{x}, \boldsymbol{\xi}) = \rho_0(\mathbf{x})\delta(\boldsymbol{\xi} - \mathbf{u}_0(\mathbf{x}))$ with

$$\widetilde{f}(0, \mathbf{x}, \boldsymbol{\xi}) = \sum_{i=1}^{M} \int_{\Omega_i} \rho_0(\mathbf{x})d\mathbf{x}\delta(\mathbf{x} - \mathbf{x}_i(0))\delta(\boldsymbol{\xi} - \mathbf{u}_0(\mathbf{x}_i(0))).$$

Denote $\widetilde{f}(0, \mathbf{x}, \boldsymbol{\xi})$ in its equivalent form

$$\mathbf{w}^M(\mathbf{x}, 0) = \sum_{i=1}^{M} \boldsymbol{\varsigma}_i(0)\delta(\mathbf{x} - \mathbf{x}_i(0)).$$

Here $\boldsymbol{\varsigma}_i(0) = (\varsigma_i^{(1)}, \ldots, \varsigma_i^{(d)}, \varsigma_i^{(d+1)})(0)$, and $\varsigma_i^{(d+1)}(0) = \int_{\Omega_i} \rho_0(\mathbf{x})d\mathbf{x}$ is the mass of the ith particle, $\varsigma_i^k(0) = u_{ik}(0) \int_{\Omega_i} \rho_0(\mathbf{x})d\mathbf{x}$ is the x_k-moment ($k = 1, \ldots, d$) of the ith particle. Solving the following ODEs

$$\frac{d\mathbf{x}_i(t)}{dt} = \mathbf{u}_i(t), \qquad \frac{d\mathbf{u}_i(t)}{dt} = -\nabla_{\mathbf{x}}V, \qquad \mathbf{u}_i(t) = (u_{i1}, u_{i2}, \ldots, u_{id})(t),$$

with initial data $\big(\mathbf{x}_i(0), \mathbf{u}_0(\mathbf{x}_i(0))\big)$, one obtains a singular solution at time t

$$\mathbf{w}^M(\mathbf{x}, t) = \sum_{i=1}^{M} \boldsymbol{\varsigma}_i(t)\delta(\mathbf{x} - \mathbf{x}_i(t)), \tag{5.1}$$

where $\boldsymbol{\varsigma}_i(t) = (\varsigma_i^{(1)}, \ldots, \varsigma_i^{(d)}, \varsigma_i^{(d+1)})(t)$, and $\varsigma_i^{(d+1)}(t) = \varsigma_i^{(d+1)}(0) = \int_{\Omega_i} \rho_0(\mathbf{x})d\mathbf{x}$ is the mass of the ith particle, $\varsigma_i^k(t) = u_{ik}(t) \int_{\Omega_i} \rho_0(\mathbf{x})d\mathbf{x}$ is the x_k-moment ($k = 1, \ldots, d$) of the ith particle at time t.

Assume one wants to find computational solutions of physical observables in $\Theta \subset \mathbb{R}^d$, the final step of the particle method is to recover the point values of the density and momenta from (5.1). Three recovery methods have been compared in [4]:

AVE: The simplest way of regularizing (5.1) is to approximate it by a piecewise constant

$$\mathbf{w}(\mathbf{x}, t) = \frac{1}{|C_j|} \sum_{i=1}^{M} \boldsymbol{\varsigma}_i(t)I_{C_j}(\mathbf{x}_i(t)), \quad \mathbf{x} \in C_j.$$

Here $\{C_j\}_{j=1}^{J}$ is an auxiliary mesh consisting of non-overlapping cells such that $\Theta = C_1 \bigcup \cdots \bigcup C_J$. Note that the mesh C is different from the mesh Ω, it should be coarser than Ω, otherwise the numerical solution will be very oscillatory.

CONV: This is the most widely used way of regularizing (5.1). Taking a convolution product with a smooth kernel $\zeta_\epsilon(x)$:

$$\mathbf{w}(\mathbf{x}, t) = (\mathbf{w}^M * \zeta_\epsilon)(\mathbf{x}, t) := \sum_{i=1}^{M} \varsigma_i(t) \zeta_\epsilon(\mathbf{x} - \mathbf{x}_i(t)), \tag{5.2}$$

where ζ_ϵ serves as a smooth approximation of the delta-function with the following properties:

$$\zeta_\epsilon = \frac{1}{\epsilon^d} \zeta\left(\frac{\mathbf{x}}{\epsilon}\right), \quad \int_{\mathbb{R}^d} \zeta(\mathbf{x}) d\mathbf{x} = 1,$$

where ϵ is a positive parameter measuring the "width" of the kernel. In our experiments, we have used the Gaussian kernel for ζ.

RED: This recovery procedure is based on the particle weights redistribution technique typically used in the immersed boundary method, [25]. For example, in the 2D numerical experiments of [4], the computational domain was divided into uniform Cartesian cells of size $\Delta x \times \Delta y$ and M particles were placed into the middle of each cell, then the point values of $\mathbf{w}$ have been computed at the equally spaced points where the particles were initially placed, namely:

$$\mathbf{w}(x, y, t) = \frac{1}{\Delta x \Delta y} \sum_{i=1}^{M} \varsigma_i(t) \phi\left(\frac{|x - x_i(t)|}{\Delta x}\right) \phi\left(\frac{|y - y_i(t)|}{\Delta y}\right),$$

where

$$\phi(r) = \begin{cases} \frac{1}{8}\left(3 - 2r - \sqrt{1 + 4r - 4r^2}\right), & |r| < 1 \\ \frac{1}{8}\left(5 - 2r - \sqrt{-7 + 12r - 4r^2}\right), & 1 < |r| < 2 \\ 0, & \text{otherwise.} \end{cases}$$

5.2. Numerical examples. EXAMPLE 5.1. A free particle model for a Gaussian pulse: $V(x) = 0$. The initial data is taken to be $f(0, x, \xi) = \rho_0(x)\delta(\xi - u_0(x))$, where $\rho_0(x) = \exp(-(x - 0.5)^2)$, and $u_0(x) = -\sin(\pi x)|\sin(\pi x)|$. This example is taken from [10]. We plot the solutions at time $t = 1$, "OUR" indicates the numerical solution obtained by our method, "AVE/CONV/RED" indicates the numerical solutions obtained by the "AVE/CONV/RED" recovery procedures. In these four methods, the time step is taken to be $\Delta t = \Delta x/5$, where $\Delta x = 2/N$, N is the number of particles.

We show the multi-valued solutions $\widetilde{u}$ and $\widetilde{\rho}$ at time $t = 1$ obtained by our method with $N = 400$ in Figure 5.1. One can compare them with Figures 7, 8 and 9 in [10] which are numerical solutions of this problem obtained by the moment methods, and our method yields much better numerical solutions.

We also compare our result with solutions obtained by previous particle methods. One can see in Fig 5.2, that the solutions obtained by AVE and RED methods are oscillatory. Fig 5.2 also shows that our solution is much better than the CONV solution, especially around the caustics. Fig 5.3 shows the comparison between our
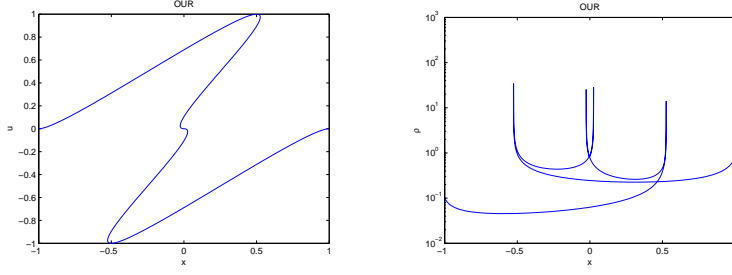
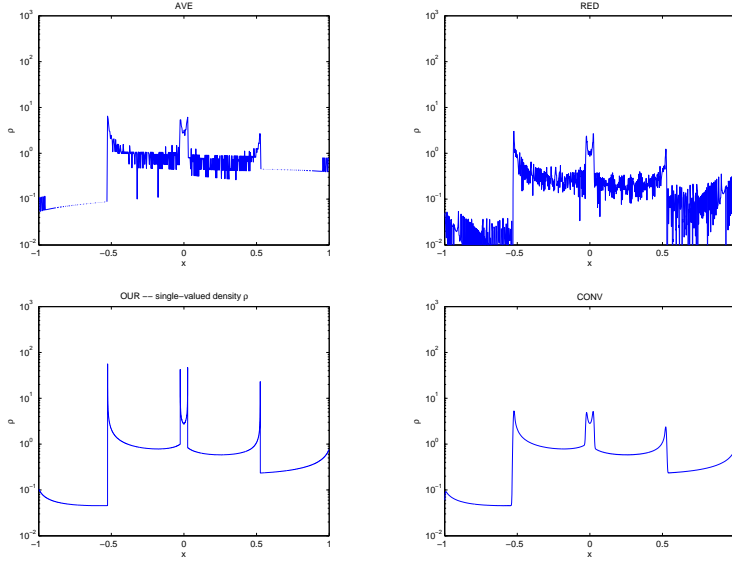Fig. 5.1: Ex5.1, new method with 400 particles, left:velocity $\widetilde{u}$, right:density $\widetilde{\rho}$, t=1.

Fig. 5.2: Ex5.1, single-valued density ρ with 1000 particles, t=1.

solution and exact solution which is obtained by taking Δx and Δt very small. One can see that they match very well.

When using the CONV method, one has to choose the width of the Gaussian kernel. We show solutions for different choices of the width in Fig 5.4. One can see that for large width ϵ, the solution is severely smeared, while for small ϵ, the solution becomes oscillatory. The best choice turns out to be 0.004 for this example. No formula has been given on how to choose ϵ for general problems. Our solution outperforms the CONV method even with the best choice $\epsilon = 0.004$.

EXAMPLE 5.2. In this example (taken from [4], example 4.3), the initial data are given by $f(0, x, \xi) = \rho_0(x)\delta(\xi - u_0(x))$, where $\rho_0(x) = 1$, $u_0(x) = 1 - 0.5 \arctan(20x)$, and the potential is $V(x) \equiv 0$. We compute the solution with $N = 400$ and output the solution at $t = 0.4$. In [4] AVE, RED and CONV particle methods were been used with the same particle number $N = 400$ (figures 5 and 6, page 574). The AVE and RED solutions are very oscillatory, while the CONV method with the best choice of $\epsilon = 0.1\sqrt{0.005}$ yields a better solution but still has oscillation. If one doubles ϵ, then it is oscillation-free, but the peaks in the density are much lower, i.e., peaks equal 5
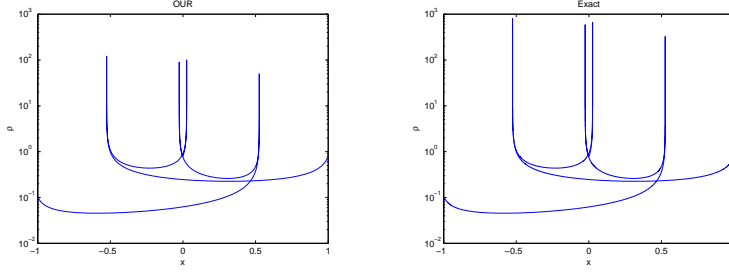
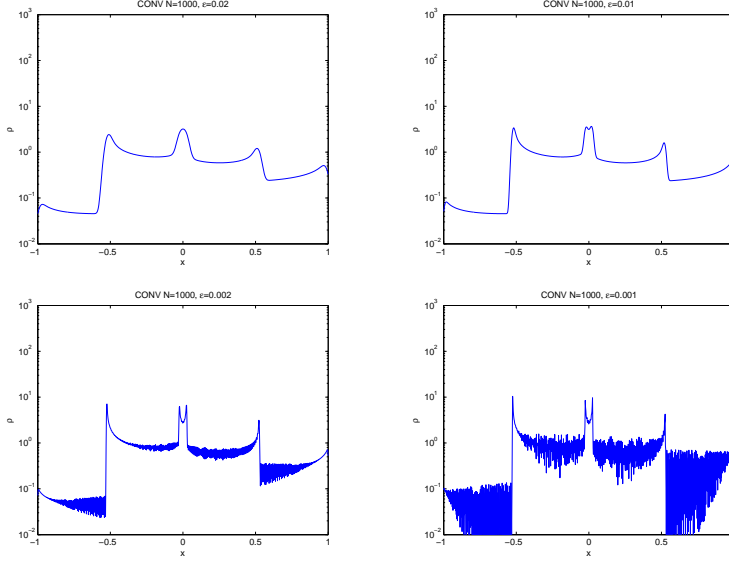Fig. 5.3: Ex5.1, multi-valued $\widetilde{\rho}$ at t=1, left:OUR with 1000 particles, right:exact.

Fig. 5.4: Ex5.1, ρ obtained by CONV with 1000 particles with different ϵ, t=1.

for bigger ϵ and 6 for smaller ϵ. Our method yields much better results: our solutions are oscillation-free, much more accurate at peaks – the peak value of our solution is around 70. See Figures 5.5 and 5.6.

The following examples are numerical solutions of the Vlasov-Poisson equations. We compare our method with the CONV particle method. The main difference of the two methods is: in our method, we use (3.4) and (3.5) to calculate the local density ρ on *uniform mesh points* in each time step, then solve the Poisson equation; in CONV, we use (5.2) to calculate the local density ρ on *uniform mesh points* in each time step.

EXAMPLE 5.3.   We solve the 1D Vlasov-Poisson equations with periodic initial data $f_0 = \delta(v - \sin(2\pi x))$,

$$\frac{\partial f}{\partial t} + v\frac{\partial f}{\partial x} - E(x,t)\frac{\partial f}{\partial v} = 0, \ \frac{\partial^2}{\partial x^2}V = \int_{-\infty}^{\infty} f(x,v,t)dv - 1, \ E = -\frac{\partial V}{\partial x}.$$

We compare density ρ, and electric field E obtained by different methods with different particle numbers N at $t = 0.5$. When solving the Poisson equation, we take the boundary condition $V(0) = V(1) = 0$. We take $\Delta t = \Delta x = 1/N$. The results are
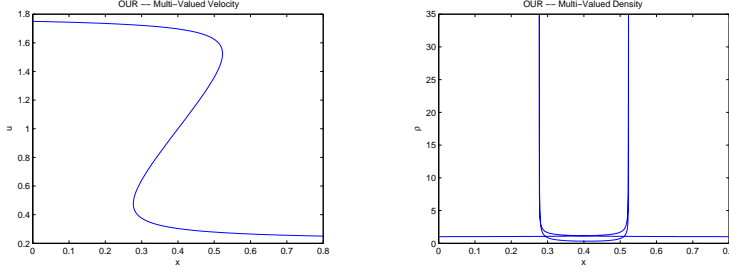
Fig. 5.5: Ex5.2, left:multi-valued velocity $\widetilde{u}$, right:multi-valued density $\widetilde{\rho}$, t=0.4.
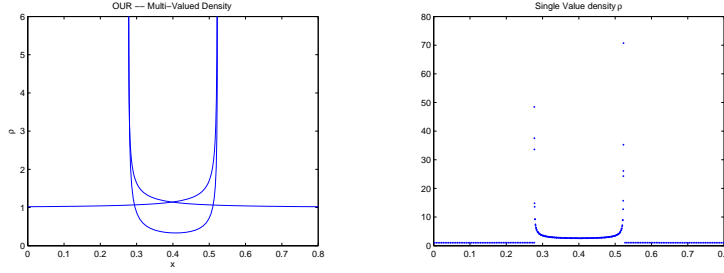

Fig. 5.6: Ex5.2, t=0.4, left: multi-valued $\widetilde{\rho}$ zoomin, right: single-valued density ρ.

shown in Figs 5.7.

One can see that our method yields much better solutions for the density ρ and electric field E. Furthermore, when apply the CONV method, for each N, we do serval tests for different widths of the Gaussian kernel ϵ, and show the best in our graphs. Hence, our method outperforms the best that a CONV method can do, especially when N is small.

EXAMPLE 5.4. We solve the 2D Vlasov-Poisson equation (4.1) with initial data

$$f(0, \mathbf{x}, \boldsymbol{\xi}) = \rho_0(\mathbf{x})\delta(\boldsymbol{\xi} - \mathbf{u}_0(\mathbf{x})),$$

where

$$\rho_0 = I_{|\mathbf{x}-(1,1)|<0.75}, \quad \mathbf{u}_0 = 2\sin\left(4\pi\big|\frac{4}{3}\big(\mathbf{x} - (1,1)\big)\big|^{5/6}\right)\big(\mathbf{x} - (1,1)\big)\Big/3|\mathbf{x} - (1,1)|.$$

We calculate the solution on spatial domain $[0,2] \times [0,2]$. The initial particles are placed inside $[-0.75, 0.75] \times [-0.75, 0.75]$, with $\Delta x = \Delta y = 1.5/N$. The uniform meshes for the Poisson equation are on domain $[0,2] \times [0,2]$ with $\Delta x = \Delta y = 2/N$. Δt is chosen to be $1/2N$. When solving the Poisson equation, we take the following boundary condition

$$V(0, \cdot) = V(2, \cdot) = V(\cdot, 0) = V(\cdot, 2) = 0.$$

The initial velocity profile is shown in Fig 5.8. For short times, if one ignores the Poisson potential, one can still gain some information (such like the basic shape) of the velocity profile. The velocity at $t = 0.2$ without involving the Poisson potential is shown in Fig 5.8, which suggests that for the Vlasov-Poisson equations of this example four caustics will form at $t = 0.2$.
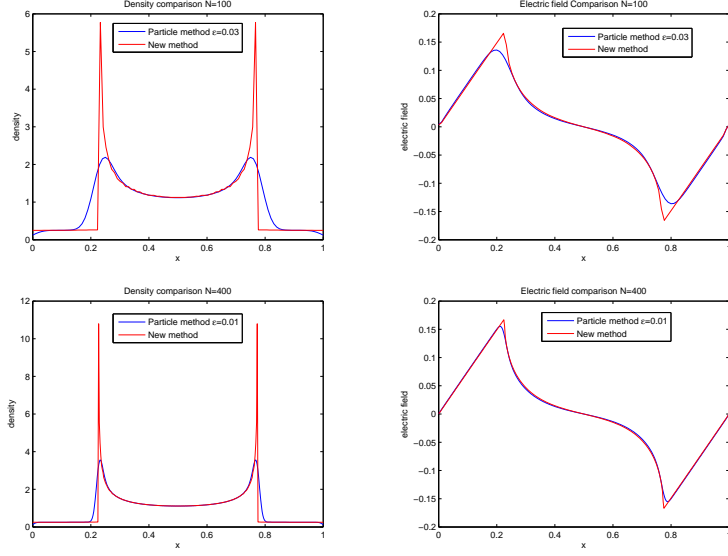
Fig. 5.7: Ex5.3, left: density ρ, right: electric field E.
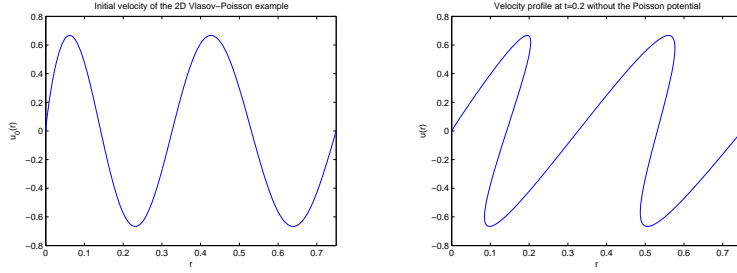
Fig. 5.8: Ex5.4, left: $u_0(r)$, right: velocity at t=0.2 without the Poisson potential.

We compare the density ρ and potential V obtained by our method and the CONV particle method with different N at $t = 0.2$. The results are shown in Figs 5.9, 5.10, and 5.11. The time cost for each method with different N are listed in Table 5.1. Roughly speaking, with the same particle number, the time cost of the new method is approximately 1/10 of the CONV particle method. The largest local density near the caustics that obtained by the new method and the CONV particle method are listed in Table 5.2. Combine these results, we can say that compared with the CONV particle method our new method yields better numerical results with less computational cost.

6. Concluding remarks. In this paper, we proposed a new numerical method for the semiclassical limit of the Schrödinger equation (the Liouville equation with measure-valued initial data) and Vlasov-Poisson equations. Our method constructs the local density based on a conservative quantity–the charge. Therefore it avoids the smoothing procedures of the previous particle methods. Numerical examples verify that compared with the previous particle methods our method yields better numerical solutions with less computational cost.

	$N = 50$	$N = 100$	$N = 150$	$N = 200$	
New method	40	807		17493	(seconds)
CONV method	435	10735	113318		(seconds)

TABLE 5.1

Ex5.4, comparison of the time cost of the new and CONV method.

	$N = 50$	$N = 100$	$N = 150$	$N = 200$
New method: $\max \rho$	12.6083	21.3102		80.3682
CONV method: $\max \rho$	1.9091	2.3927	2.9320	

TABLE 5.2

Ex5.4, comparison of $\max \rho$ of the new and the CONV method.

REFERENCES

[1] C.K. Birdsall, A.B. Langdon, Plasma Physics via Computer Simulation, Adam Hilger, New York, 1991.

[2] F. Bouchut, Global weak solution of the Vlasov-Poisson system for small electrons mass, Comm PDEs, 16, 1337-1365, 1991.

[3] L.-T. Cheng, H.-L. Liu and S. Osher, Computational high-frequency wave propagation using the Level Set method, with applications to the semi-classical limit of Schrödinger equations, Comm. Math. Sci. 1, 593-621, 2003.

[4] A. Chertock and A. Kurganov, Computing multivalued solutions of pressureless gas dynamics by deterministic particle methods, Commun. Comput. Phys. no. 2-4, 565-581, 2009.

[5] A.J. Chorin, Numerical study of slightly viscous flow, J. Fluid Mech. 57, no. 4, 785796, 1973.

[6] G.-H. Cottet and P.D. Koumoutsakos, Vortex Methods, Cambridge University Press, Cambridge, 2000.

[7] B. Engquist and O. Runborg, Computational high frequency wave propagation, Acta Numer. 12, 181-266, 2003.

[8] F. Filbet, E. Sonnendrcker, P. Bertrand, Conservative numerical schemes for the Vlasov equation, Journal of Computational Physics, 172, 166 187, 2001.

[9] P. Gerard, P.A. Markowich, N.J. Mauser, and F. Poupaud. Homogenization limits and Wigner transforms, Comm. Pure Appl. Math., 50(4), 323-379,1997.

[10] L. Gosse, S. Jin and X. Li, On two moment systems for computing multiphase semiclassical limits of the Schrödinger equation, Math. Model Mech. Appli. Sci. 13, 1689-1723, 2003.

[11] R. Hockney, J. Eastwood, Computer Simulation Using Particles, Institute of Physics Publishing, 1988.

[12] S. Jin and X.T. Li, Multi-phase computations of the semiclassical limit of the Schrödinger equation and related problems: Whitham vs Wigner, Physica D, 182, 46-85, 2003.

[13] S. Jin, P.A. Markowich and C. Sparber, Mathematical and computational methods for semiclassical Schrödinger equations, Acta Numerica 20, 121-289, 2011.

[14] S. Jin, H.L. Liu, S. Osher and R. Tsai, Computing multi-valued physical observables for high frequency limit of symmetric hyperbolic systems, J. Comp. Phys. 210, 497-518, 2005.

[15] S. Jin and K. Novak, A semiclassical transport model for thin quantum barriers, Multiscale Modeling and Simulation, 5(4), 1063-1086, 2006.

[16] S. Jin and K. Novak, A semiclassical transport model for two-dimensional thin quantum barriers, J. Comp. Phys. 226, 1623-1644, 2007.

[17] S. Jin and S. Osher, A level set method for the computation of multi-valued solutions to quasilinear hyperbolic PDE's and Hamilton-Jacobi equations, Comm. Math. Sci. 1(3), 575-591, 2003.

[18] N.A. Krall and A.W. Trivelpiece, Principles of Plasma Physics, San Francisco Press, 1996.

[19] P.L. Lions and T. Paul, Sur les measures de Wigner, Revista. Mat. Iberoamericana 9, 553-618, 1993.

[20] P.L. Lions and B. Perthame, Propagation of moments and regularity for the 3-dimensional Vlasov-Poisson system, Inventiones Mathematicae, 105, 415-430, 1991.

[21] A. Majda, G. Majda and Y.X. Zheng, Concentrations in the one-dimensional Vlasov-Poisson equation I: Temporal development and non-unique weak solutions in the single component case, Physica D, 74, 268-300, 1994.
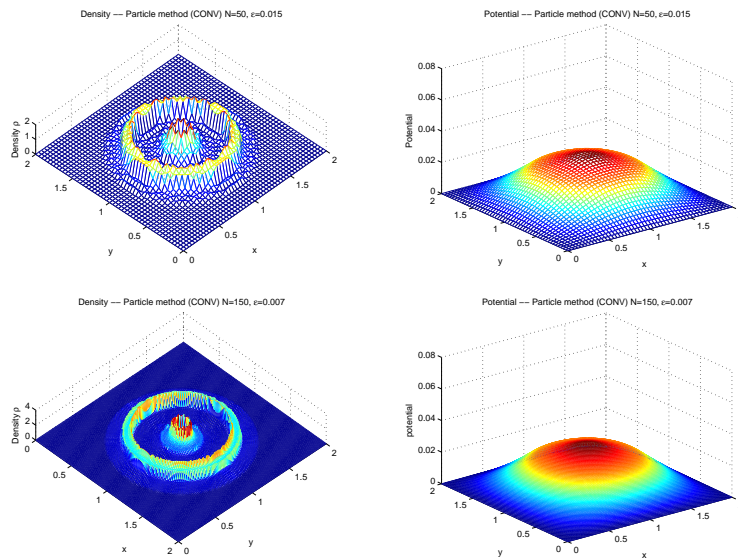
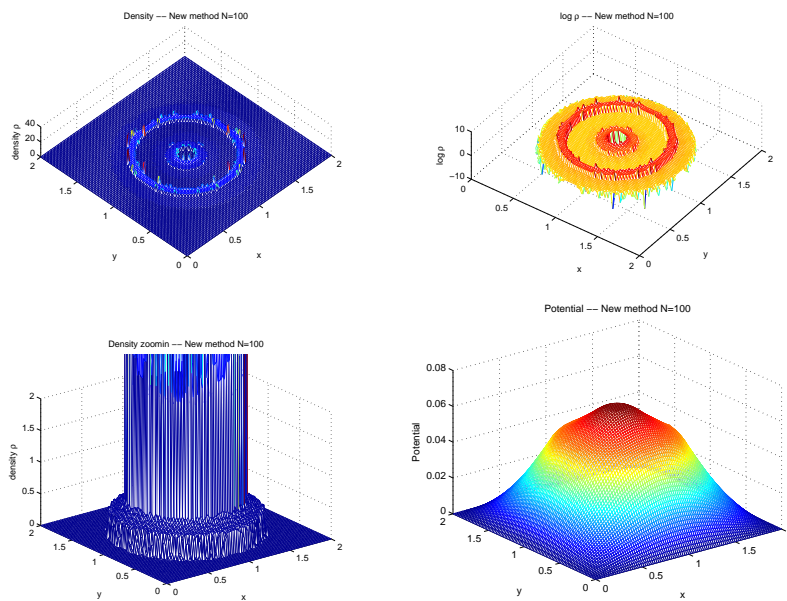Fig. 5.9: Ex5.4, the CONV particle method with different N and ϵ.

Fig. 5.10: Ex5.4, New method, N=100.

[22] A. Majda, G. Majda and Y.X. Zheng, Concentrations in the one-dimensiolal Vlasov-Poisson e-
     quations. II: Screening and the necessity for measure-valued solutions in the two component
     case, Physica D, 79, 41-76, 1994.
[23] P.A. Markowich and C.A. Ringhofer, Semiconductor Equations, Springer, 1990.
[24] S. Osher, L.-T. Cheng, M. Kang, H. Shim and Y.-H. Tsai, Geometric optics in a phase-space-
     based level set and Eulerian framework, J. Comput. Phys. 179(2), 622-648, 2002.
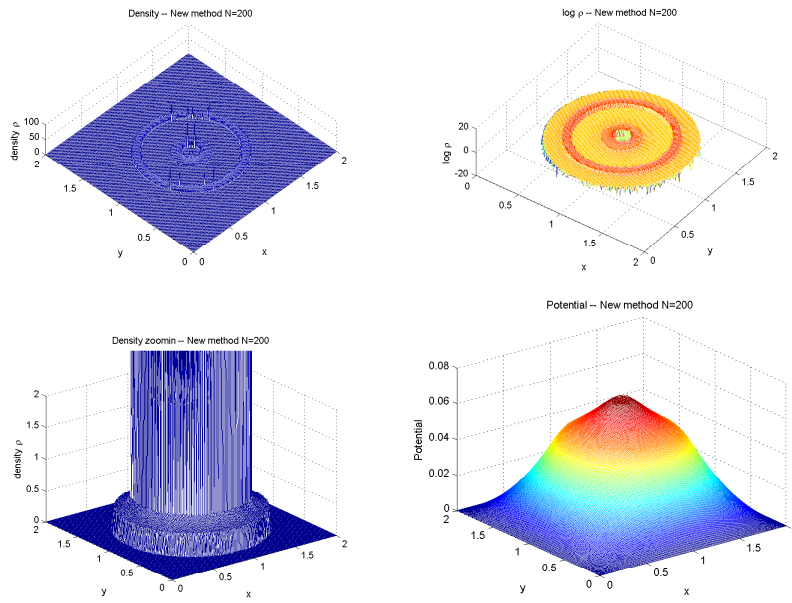[25] C.S. Peskin, The immersed boundary method, Acta Numer. 11, 479-517, 2002.

Fig. 5.11: Ex5.4, New method, N=200.

[26] P.-A. Raviart, An analysis of particle methods, Numerical Methods in Fluid Dynamics (Como, 1983), Lecture Notes in Math., vol. 1127, Springer, Berlin, 243324, 1985.

[27] C. Sparber, P. Markowich and N. Mauser, Wigner functions versus WKB methods in multivalued geometrical optics, Asymptot. Anal. 33(2), 153-187, 2003.

[28] J. Vay, P. Colella, P. Mccorquodale, B. Van Straalen, A. Friedman, D. Grote, Mesh refinement for particle-in-cell plasma simulations: applications to and benefits for heavy ion fusion, Laser and Particle Beams, 20, 569575, 2003.

[29] J. Verboncoeur, Particle simulation of plasmas: review and advances, Plasma Physics and Controlled Fusion, 47 (2005) 46.

[30] D. Wei, 1D Vlasov-Poisson equations with electron sheet initial data, Kinetic and Related Models, Volume 3, Number 4, 729-754, 2010.

[31] Y.X. Zheng and A. Majda, Existence of global weak solutions to one-component Vlasov-Poisson and Fokker-Planck-Poisson systems in one space dimension with messures as initial data, Comm. on Pure and Applied Math. Vol. XLVII, 1365-1401, 1994.